Original Article

J Strain Analysis
0(0) 1–10

DOI: 10.1177/0309324711434681
sdj.sagepub.com
SAGE

Effects of the weld groove shape and geometry on residual stresses in dissimilar butt-welded pipes

Davood Akbari, Mohammadreza Farahani and Naser Soltani

Abstract

The thermo mechanical behavior of the welding process was analyzed using the finite element technique to determine the residual stress magnitude and distribution in butt-welded pipes. An efficient user subroutine was developed in a finite element model to consider the effects of phase transformation in the analysis. The calculated results verified using the determined data presented by Deng for similar weld joints and measured data by the hole drilling technique for dissimilar weld joint.

Good correspondence between the finite element results and experimental data infers that the computational procedure developed in this study is an effective method for residual stress prediction in dissimilar welded joints. The effects of pipe wall-thickness, weld groove angle and root opening distance on welding residual stresses in dissimilar butt-welded pipes were studied using the prepared finite element model. It is observed that the pipe wall-thickness has important influences on the residual stress magnitude and distribution. Meaningful influences from weld groove angles and root opening distances are observed on the axial residual stresses in the ferritic side.

Keywords

Residual stresses, hole drilling method, dissimilar butt-weld, pipe thickness, groove angle, root opening distance

Date received: 28 June 2011; accepted: 9 December 2011

Introduction

In many industrial applications, including chemical and petrochemical installations, power generation, and the pulp and paper industry, it is necessary to weld ferritic steels to austenitic ones. Initially, the joints must meet the strength requirements, while the anticorrosive properties are also of importance. However, residual stresses and distortions can occur near the weld bead due to localized heating during the welding process and the subsequent rapid cooling.

In some cases, welding residual stresses can have a deleterious effect on the mechanical properties of the joints, e.g. brittle fracture resistance and fatigue performance.[1]

It is demonstrated that the dissimilar weld joints fail in less than their expected service life. A majority of the transition joint failures, in austenitic/ferritic steels joints occur in the heat affected zone of the ferritic steel, adjacent to the weld interface. In power plants, there is strong evidence that the residual stresses are the major causes of cracking in welds and HAZ regions during service.[2] Therefore, estimating the welding residual stress magnitude and distribution and characterizing the effects of certain welding conditions on the residual stresses in dissimilar weld joints are relevant tasks.

Several parameters may affect the magnitude and distribution of the residual stresses. The welding process parameter, material properties and structural factors have significant influences on welding residual stress magnitude and distribution. Process parameters include the employed welding process type, arc traveling speed, voltage and current. The weld groove shape, weld joint type, thickness and geometry type are some of the structural factor that may affect the residual stresses in weld joint.

Investigators have developed several methods, including heat treatment, hammering, preheating and

School of Mechanical Engineering, University of Tehran, Iran

Corresponding author:
Mohammadreza Farahani, School of Mechanical Engineering, College of Engineering, University of Tehran, Kargar Shomali Street, 11155-4563, Islamic Republic of Iran.
Email: O.Farahani@gmail.com

vibration stress relieving to decrease the welding residual stresses.[3] Besides, it is possible to diminish the residual stresses attributed to welding by controlling the welding parameters. Choosing the proper welding parameters and joint design is a more simple and efficient way to reduce the residual stresses induced by welding. Post-weld measurement of residual stresses and the residual stress reduction process is not applicable for most of the welded structures; therefore, developing available welding parameters and accurately predicting the welding residual stresses for weld systems are necessary for achieving the suitable design.

Differences in mechanical properties across the dissimilar weld joints and coefficients of thermal expansion (CTE) of the two types of steels (CTE for austenitic stainless steel and ferritic steel are typically 18×10^{-6} and 14×10^{-6}/K, respectively), the resulting creep at the interface and phase transformation make the prediction of the residual stress distribution in dissimilar weld joints very difficult and complex.[2]

Nowadays, the numerical techniques can be used satisfactorily in calculating the residual stresses in welded structures. Many investigations have been done on the modeling and analysis of the thermal fields in weldments, and the investigators have tried to study the effects of some of the above parameters on the thermal history of the welded parts. Different models were developed to simulate the inserted heat of the welding arc into the weldments. For example, in 1984, Goldak et al.[4] presented a new finite element method to determine the thermal history of the weld. They used the heat flux approach for their modeling. Goldak also modeled the thermal stresses in the welded structures.[5]

Numerical analyses and experimental studies carried out by Mochizuki et al. in order to predict the residual stresses in carbon steel pipes.[6] They verified their numerical models using the neutron diffraction residual stress measurement technique. Peng-Hsiang et al. predicted the residual stresses during one-pass arc welding in steel plates using finite element method.[3] They also studied the effects of traveling speed, specimen size, external mechanical constraints and preheating on the residual stress magnitude and distribution. The temperature distribution in dissimilar welded plates was simulated by Elena and Mihaela.[7] The effects of heat input on the residual stress distribution of dissimilar welded pipes were investigated by Akbari and Sattari-Far.[8] Joseph et al. employed an Inconel-82 buttering layer to reduce the residual stresses in the dissimilar weld joint between 2.25Cr–1Mo ferritic steel and AISI type 316 stainless steel.[2] In their work, residual stress profiles across the weld joints were determined using the X-ray diffraction (XRD) technique.

There are very limited investigation on the influences of geometrical parameter of weld joint and the welding process parameters on the residual stress magnitude and distribution in the literature.

In this paper, dissimilar welded pipes fabricated from A106-B carbon steel and A240 TP304 stainless steel by multi-pass arc welding technique were simulated using the three-dimensional (3D) finite element simulation and the residual stress distributions were obtained. These numerically obtained results were verified using the hole drilling residual stress measurement. Then the influences of geometry parameters, e.g. wall thickness, root opening and groove angle on the magnitude and distribution of residual stresses in this joint, were also discussed with an aim to reduce the welding residual stresses by choosing the proper welding parameters and joint design.

Experimental investigation

In this study, the residual stresses in a dissimilar weld joint were measured using the hole drilling strain gauges methods. The experimental data were used to verify the obtained results by finite element analysis for the dissimilar weld joint. The experimental results presented by Deng and Murakawa were also used here to verify the result obtained in a similar weld joint from SUS304 steel (equivalent to ASTM TYPE304).[9]

Specimen preparation

In this paper, two pipes with nominal diameter of 8 in, outer diameter of 219.1 mm, thickness of 8.1 mm (Sch40 s) and length of 220 mm were prepared. A240-TP304 stainless steel and A106-B carbon steel were used here in dissimilar butt weld joint. The initial microstructure of the stainless steel TP304 was austenite and had no phase transformation in welding but the carbon steel side experienced the martensitic phase transformation during the welding process.

The prepared pipes with V groove edges are shown schematically in Figure 1.

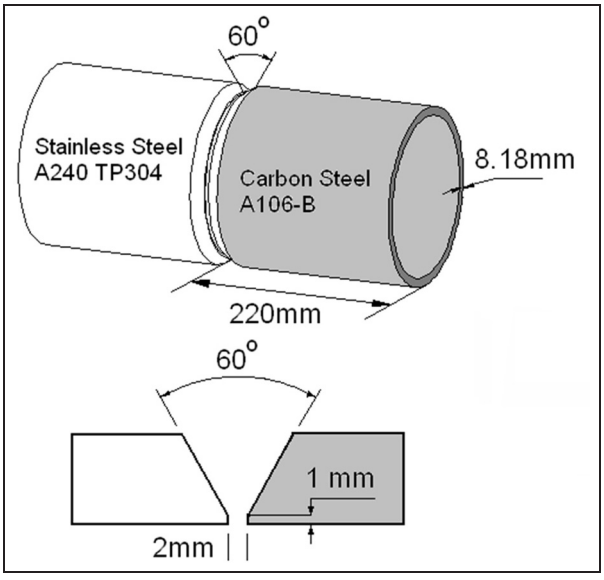

Figure 1. Schematic view of the specimen used in this experiment.

Table 1. List of the welding process parameters.

Pass sequence	Pass No.	Welding method	Filler	Welding parameters		
				Welding current I (A)	Welding voltage U (v)	Travelling speed (mm/s)
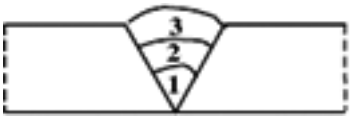	1	GTAW	ER 308L	95±5	9	0.55
	2	SMAW	E 308L-16	115±5	27-28	3.4-4.1
	3	SMAW	E 308L-16	145±5	25-28	2.7-2.8

The weld joint was fabricated in three passes. The first pass was done using the gas tungsten arc welding (GTAW) process and other passes by shield metal arc welding (SMAW) method. E308L Austenitic stainless steel was used as the filler metal. The welding parameters of each pass are presented in Table 1. Exactly the same parameters were used in the finite element simulation.

The residual stresses measurement

In this investigation, the residual stresses were measured using the hole drilling method, a standard technique which is described in ASTM E837.[10] The residual stress measurement in the dissimilar weld joint were made in eleven points, one point at the weld centre and five symmetric points at each side of the joint. Strain gauges were mounted on the outer surface of the pipes. A very high-speed drill was employed for drilling at the centre point of the strain gauges. The released strains during the hole drilling were measured. Then the maximum and minimum components of residual stresses were determined using the measured released strains by

$$\sigma_{\max} = \frac{\varepsilon_1 + \varepsilon_2}{4A} - \frac{1}{4B}\sqrt{(\varepsilon_3 - \varepsilon_1)^2 + (\varepsilon_3 + \varepsilon_1 - 2\varepsilon_2)^2} \quad (1)$$

$$\sigma_{\min} = \frac{\varepsilon_1 + \varepsilon_2}{4A} + \frac{1}{4B}\sqrt{(\varepsilon_3 - \varepsilon_1)^2 + (\varepsilon_3 + \varepsilon_1 - 2\varepsilon_2)^2} \quad (2)$$

where $\varepsilon_1, \varepsilon_2, \varepsilon_3$ are the measured strains and A and B are two coefficients depend on the hole diameter and base metal mechanical properties.[10] Figure 2 shows the residual stresses measurement by the hole drilling method. To avoid the effects of starting and ending points of arc welding, measurements were accomplished in the farthest point from the discontinuity in the pipe joint.

Figure 2. Residual stress measurement by the hole drilling technique.

Finite element calculations

Welding simulation

In this study, the finite element method was used to calculate the temperature fields during the welding process and subsequently the residual stress distributions in the weld joint.

As a result of small dimensional changes in the welding process and negligible mechanical work in comparison with thermal energy of the welding, an uncoupled formulation was used to simulate the thermo-mechanical behavior of the weldment, so the thermal analysis was carried out independent from the mechanical analysis to obtain the temperature history of the welding process. During each weld pass, the thermal stresses were calculated from the temperature distribution determined by the thermal model. The stresses in each temperature increment were added to the nodal point locations to update the behavior of the model before the next increment. Due to non-linearity in the mechanical analysis of the welding process, the full Newton–Raphson method was used here.

The weldment and base metals properties were assumed to be temperature dependent as presented in Figure 3. The element birth and death technique was used in this study for simulating the filling metal deposition during the welding. In this technique, first the filler metal elements were deactivated using a very small factor multiplied to their stiffness matrixes. Deactivated elements were activated again during the welding process step by step, by moving the welding heat source.

A sensitivity analysis of mesh sizes was conducted to confirm the robustness of the mesh. The finite element mesh used in this modeling for the weld joint simulation is shown in Figure 4.

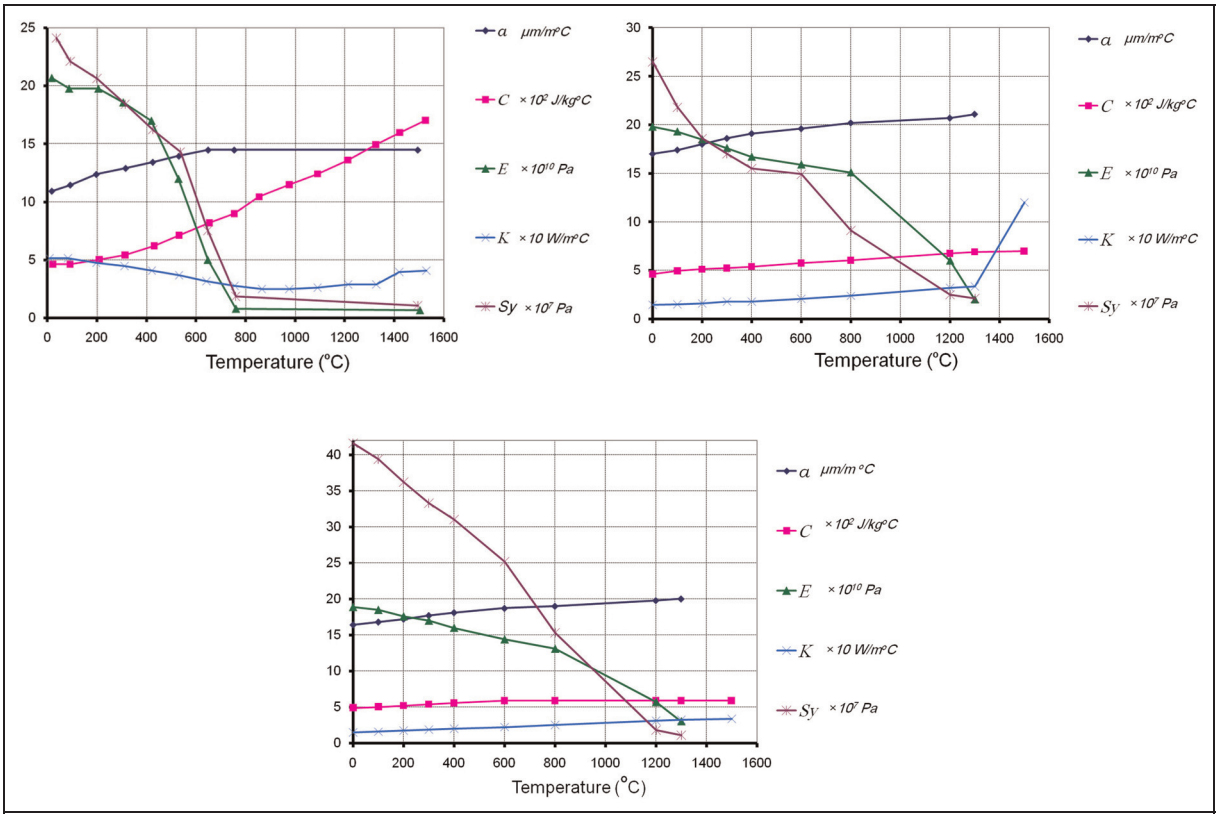

Figure 3. Material properties of A106-B carbon steel[1] and A240 TP 304 stainless steel[11] and Filler metal E308L versus temperature.

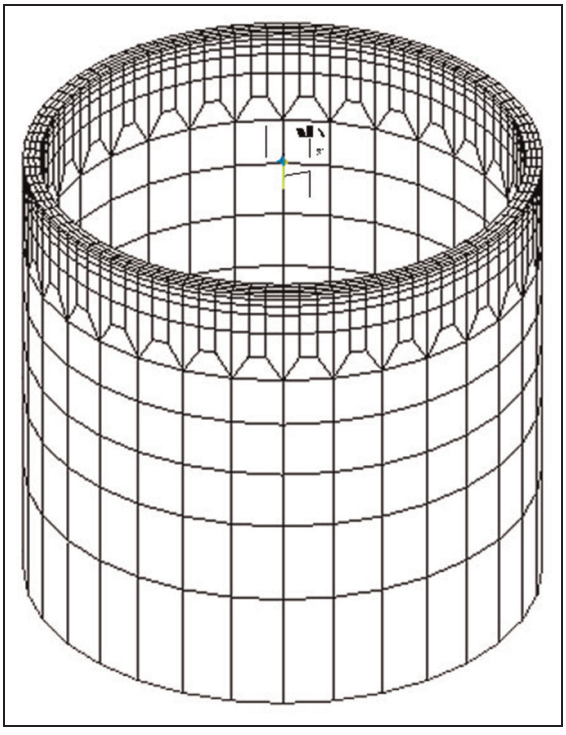

Figure 4. Half of the finite element meshes for the welded pipes.

Thermal analysis

Thermal analysis was used to determine the temperature distributions of the welded parts. The governing equation of the transient heat transfer during this process is given by[9]

$$\rho c \frac{\partial T}{\partial t}(x, y, z, t) = -\nabla.\vec{q}(x, y, z, t) + Q(x, y, z, t) \quad (3)$$

where T, t, $\vec{q}$ and Q are the temperature, time, the heat flux vector and the internal heat generation rate respectively. And also ρ is the density, c is the specific heat capacity, ∇ is the spatial gradient operator and x, y and z are the coordinates.

A double ellipsoidal distribution suggested by Goldak et al. was used in this study to model the volumetric heat source of the arc welding process. The Goldak heat source distribution, as is shown in Figure 5, is expressed by the following equations[9,12]

$$q_f(x, y, z) = \frac{6\sqrt{3} f_f Q}{a_f bc\pi^{3/2}} e^{(-3x^2/a_f^2)} e^{(-3y^2/b^2)} e^{(-3z^2/c^2)} \quad (4)$$

$$q_r(x, y, z) = \frac{6\sqrt{3} f_r Q}{a_r bc\pi^{3/2}} e^{(-3x^2/a_r^2)} e^{(-3y^2/b^2)} e^{(-3z^2/c^2)} \quad (5)$$

where equations (4) and (5) represent the front and rear part of the heat source, respectively. In these equations x, y and z are the local coordinates of the heat source and f_f and f_r are parameters which give the fraction of the heat deposited in the front and the rear parts, respectively. Q is the power of the welding heat source which can be obtained from the experimental welding process data. The parameters a, b and c are related to

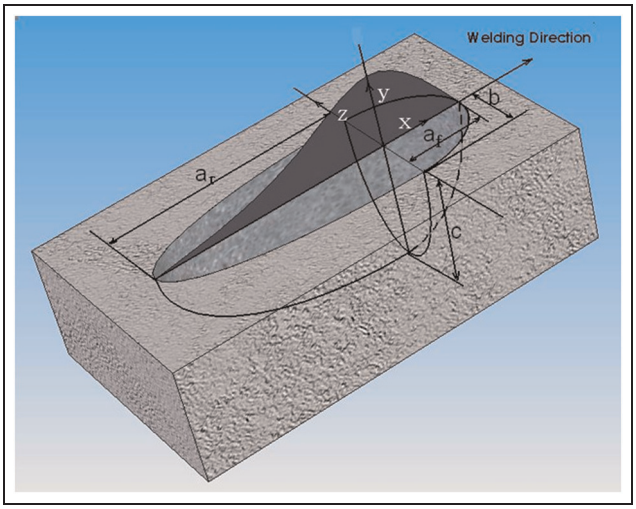

Figure 5. Double ellipsoid heat source configuration.

the cross-sectional dimensions of the welding heat source that are shown in Figure 5. If the cross-sectional dimensions of the weld joint are not available, the experience data given by Goldak et al. suggest that it is reasonable to take the distance in front of the heat source equal to one-half of the weld width and the distance behind the heat source equal to twice the weld width.[12] These suggestions were used in this paper and the moving heat source was modeled by generating a user subroutine in finite element model in ANSYS.[13]

Welding parameters used in this analysis were based on the experimental measured data given in Table 1. During the welding process, the heat losses included radiation dominated at the weld zone and convection dominated away from the weld, so the total heat transfer coefficient is considered as:[9,11]

$$\left\{ \begin{array}{l} \alpha_h = 0.0668\ T\ (w/m^2)\ 0 < T < 500c^\circ \\ \alpha_h = 0.231T - 82.1\ (w/m^2)\ 500 < Tc^\circ \end{array} \right\} \quad (6)$$

that w stands for watts. This method is applied using a developed user subroutine for finite element simulation.

The thermal conductivity of the melted zone was doubled to simulate the influences of the weld pool fluid flow.[14] The latent heat of the fusion was considered to model the thermal effects of the weld pool solidification. Thermal enthalpy method was used here to handle the latent heat in the thermal analysis in the finite element simulation.[13]

The element type that was used for thermal modeling has a 3D thermal conduction capability. This element has eight nodes with a single degree of freedom, temperature, at each node and the isotropic material properties.

Mechanical analysis

For the mechanical analysis, the thermal elements of the model were replaced by the mechanical ones and the temperature history computed in the thermal analysis was imposed as a temperature load at each time-step in the mechanical analysis. So at each time-step, the thermal strains and stresses were calculated.

An eight nodes element with three degrees of freedom at each node: translations in the nodal x, y, and z directions and with a reduced integration scheme was employed in the mechanical analysis. The element has plasticity, creep, stress stiffening, large deflection, and large strain capabilities.

Martensite transformation in the carbon steel side was modeled by changing the yield strength of the base metal and considering the volume changes due to the phase transformation. The volume fraction of the martensite was found during the thermal analysis using the Koistinen–Marburger relationship.[15] This transformation was taken into account in mechanical analysis using a developed user subroutine in this study. Figure 6 shows the volume changes and yield strength variations due to the martensite transformation versus the temperature.[16]

The total strain in the welding process is the sum of the elastic, plastic and thermal strains and strains due to volume changes.

The temperature-dependent material properties such as Young's modulus, Poisson's ratio and thermal expansion coefficient were used in the mechanical analysis to calculate the elastic and thermal strains. In addition, the temperature dependent yield strength with the Von Mises yield criteria was used in the mechanical model to calculate the plastic strains.

As the material around the weld zone undergoes both loading and unloading in the course of the welding process, the linear kinematic hardening was also taken into account as an important feature.[17]

The strains due to volume changes were considered by modifying the thermal expansion coefficient using a developed user subroutine in ANSYS.

Due to symmetry in the geometry of the similar pipe joint (the first model), only one half of the weld joint was modeled and a symmetry boundary condition at the mid surface of the weld joint was applied. However, for the dissimilar model (the second model) the pipe joint should be modeled completely. As the forces and residual stresses are internal and self-equilibrium, it is not necessary to use any external boundary condition or constraint and only one node was fixed to prevent from rigid body motion.

FEM verification

To confirm the accuracy of the present finite element modeling, at the first step, the results of this analysis for a similar weld joint were compared with the experimental measured data presented by Deng and Murakawa.[9] Thus the FE analysis of a pipe weld joint made of SUS304 steel with the same parameters as used by Deng was directed. It should be noted that SUS304 is an austenitic stainless steel that have no martensite transformation during the welding.

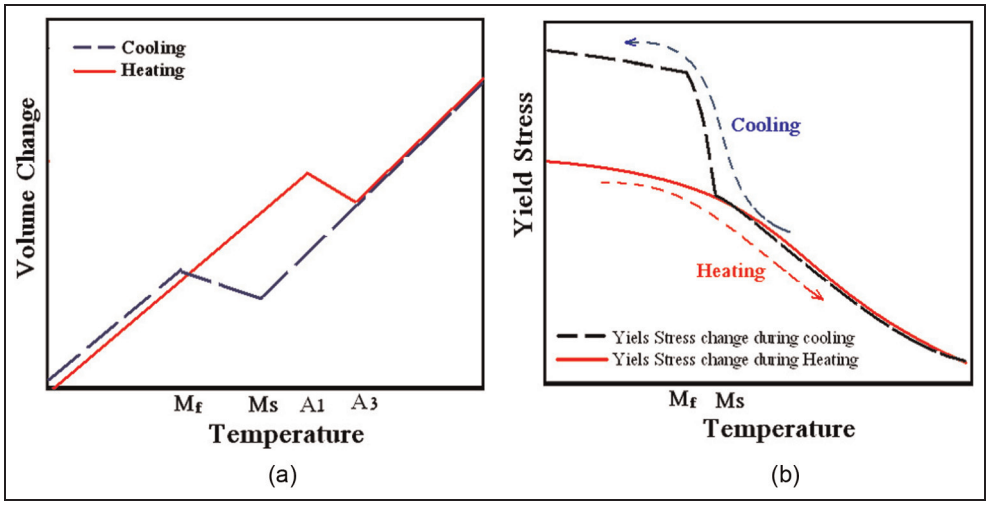

Figure 6. Schematic diagram of (a): volume changes, (b) yield strength variations, due to martensite transformation.

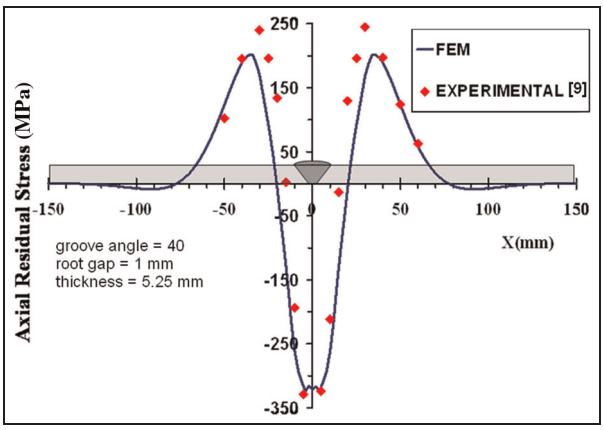

Figure 7. Axial residual stresses on the outer surface of pipes in axial direction.

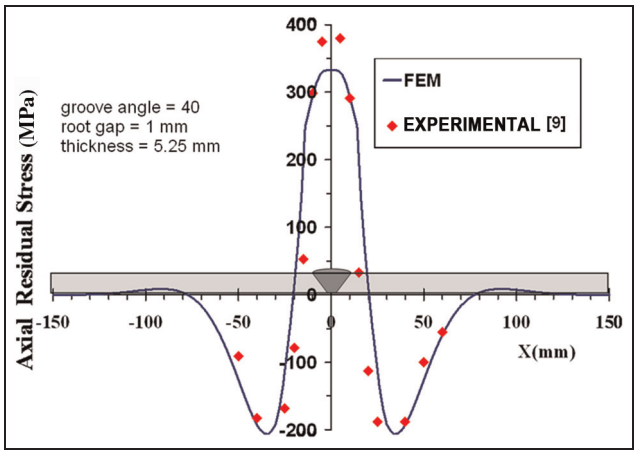

Figure 8. Axial residual stresses on the inner surface of pipes in axial direction.

Figures 7 and 8 show the axial stresses on the outer and inner surface of the welded pipe respectively. In such thin walled pipes, the axial residual stresses near the weld zone are created as a result of shrinkage in hoop direction after weldment solidification and are matched with bending profile through the thickness.

Good coincidence between the finite element and experimental result was observed, indicated that the developed finite element model can predict the welding residual stresses in similar weld joints accurately.

Figure 9 shows the hoop residual stresses on the inner surface of the welded pipe. It is observed that there is a very good agreement between the FE results and experimental results obtained by Deng.[9] Small differences between FE and experimental results may be due to the lack of enough accurate material properties data of the weldment especially in high temperature.

For the second study, the dissimilar welded joint described previously was prepared and its residual stresses were measured using hole drilling method. The residual stress distribution in the dissimilar welded joint was also calculated using finite element simulation. The finite element results in the dissimilar welded pipes, prepared in this study, were compared with the measured data as shown in Figures 10 and 11. The hoop and axial welding residual stresses are presented respectively. The measurement results using hole drilling method are presented by solid points.

Good coincidence between the finite element and experimental result was observed again. An asymmetric residual stress distribution was observed due to difference of material properties in each side of the dissimilar weld joint. It can be concluded that the current finite element model, gave a more or less reliable prediction of the welding-induced residual stresses in this dissimilar butt-welded pipe. So the parametric studies can be conducted using this validated model.

Effects of the wall thickness

Residual stresses are estimated for multi-pass dissimilar weld joints for four different pipe wall thicknesses

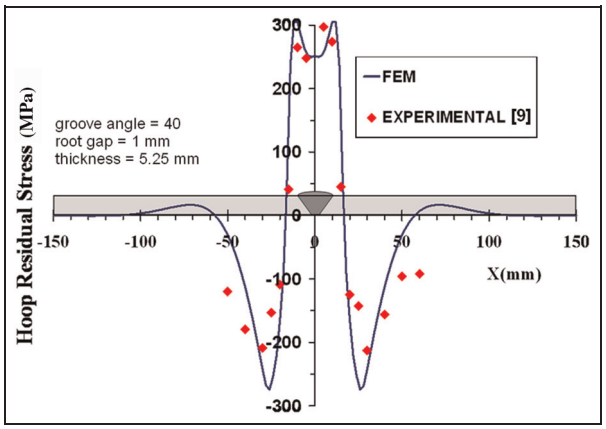

Figure 9. Hoop residual stresses on the inner surface of pipes in axial direction.

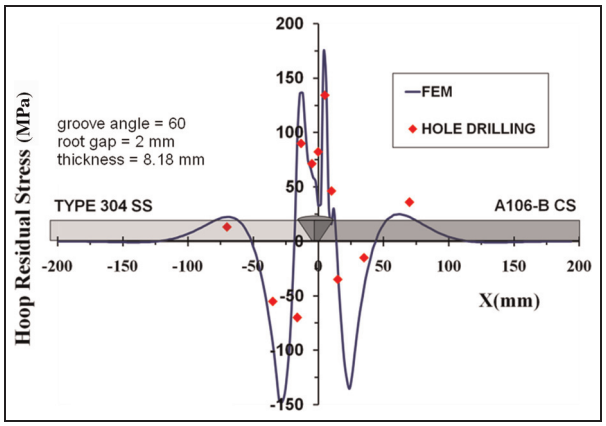

Figure 10. Hoop residual stresses on the outer surface of pipes in axial direction.

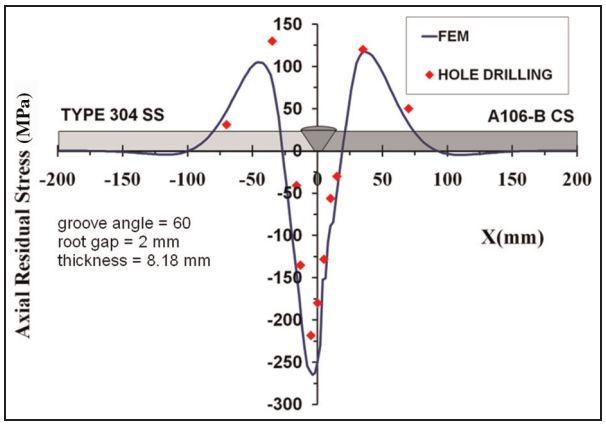

Figure 11. Axial residual stresses on the outer surface of pipes in the axial direction.

according to Table 2. All pipes have the same nominal size (as used in the experimental measurement) but different thicknesses. FE analyses have then been conducted using the validated model described before. However, as the thickness range of the models is

Table 2. Pipe wall thicknesses used in FE analysis.

Case no.	Description			
	Pipe nominal size	OD (mm)	Designation	Pipe wall thickness (mm)
1	8 in	219.1	SCH.20	6.35
2	8 in	219.1	SCH.40S	8.18
3	8 in	219.1	SCH.80	12.70
4	8 in	219.1	SCH100	15.09

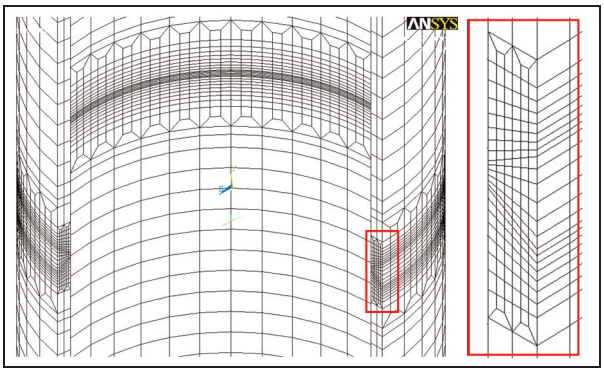

Figure 12. Finite element mesh used for pipe joint with 15 mm thickness.

significant, the element number in the thickness direction was changed for each model in order to obtain a constant mesh sizes for all models. In Figure 12, The finite element mesh for the pipe joint with 15 mm thickness is shown.

As the pipe thicknesses were not equal in each model, so the welding parameters like current, voltage and travelling speed were not constant. In order to simulate the welding process of the pipes with different thickness in three passes, the heat input of each pass was assumed to be proportional to the volume of the pass. The heat input in the experimented case (t = 8.1 mm) for each pass was calculated using measured welding parameters listed in Table 1 and equation (7) as

$$Q = \eta UI/v \tag{7}$$

where η represents the arc efficiency factor, U is the arc voltage, I is the welding current and v is the welding speed. The efficiency factor is assumed as 0.6 for the GTAW process and 0.7 for the SMAW process.

Figure 13 shows the axial residual stresses on the inner surface of four dissimilar pipes considered in this study. In general, near the weld toes for all cases, high tensile residual stresses were observed. The tensile axial residual stresses decreased away from the weldment and became compressive due to the self-balancing nature of the residual stresses.

It is observed in Figure 13 that increasing the pipe thickness did not have significant effects on the peak

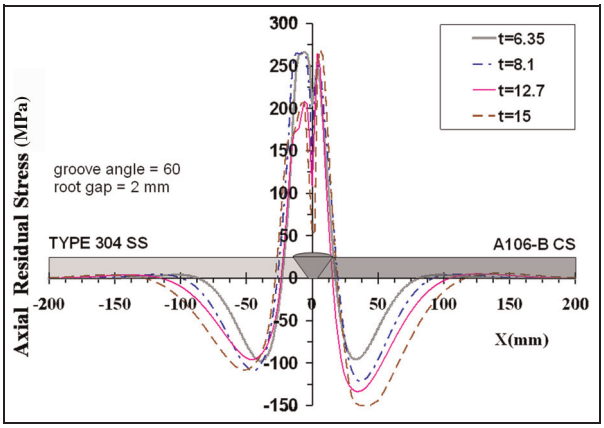

Figure 13. Axial residual stress on the inner surface for joints with different wall thicknesses.

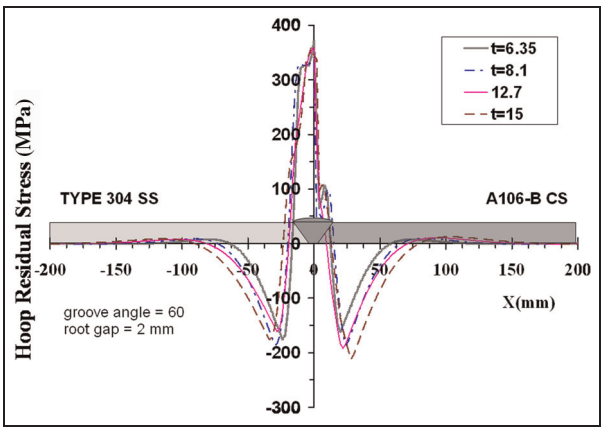

Figure 14. Hoop residual stress on the inner surface for joints with different wall thicknesses.

stress in the carbon steel side, but the peak stress in the stainless steel part decreased by increasing the pipe wall thickness. The compressive axial residual stresses on the inner surface increased by increasing the pipe wall thickness, especially in the carbon steel side. As it is shown in Figure 13, the maximum compressive stresses vary from −100 MPa in the t = 6.35 mm to −150 MPa in the t = 15 mm on the carbon steel side. Furthermore, thicker pipes had a wider distribution of compressive axial residual stresses. In the carbon steel part, compressive residual stress of −60 MPa occurred in 50 mm from the weld centre of pipes with thickness t = 6.35 mm while this stress was observed at 80 mm away from the weld centre of the pipes with thickness t = 15 mm.

Hoop residual stress distribution on the inner surface of the dissimilar joint is shown in Figure 14. The similar trend as the axial stresses is observed, but peak hoop residual stresses are higher than the axial peak stresses. It is also observed that the differences between material properties of two sides of the joint make asymmetric distribution of hoop residual stresses in the dissimilar weld joint. The peak of tensile hoop stresses has

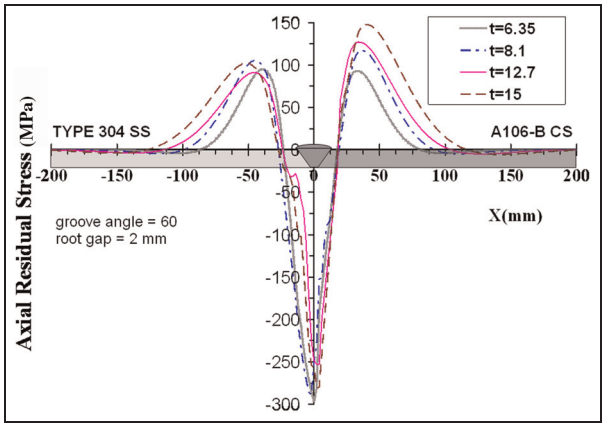

Figure 15. Axial residual stresses on the outer surface for joints with different wall thicknesses.

small changes by increasing the pipe wall thickness as it is shown in Figure 14, but the compressive hoop stresses on the inner surface increased by increasing the pipe wall thickness.

Figure 15 shows the axial residual stresses on the outer surface of the dissimilar joints along the axial direction. It is clear that the axial stresses on the outer surface are approximately reverse of the axial stresses distribution on the inner surface. It is also observed that the pipe wall thickness has a negligible effect on the peaks of the tensile axial residual stress on the outer surface at the stainless steel side. However, higher tensile residual stresses on the carbon steel side was determined for thicker pipes. In this case, peak axial residual stresses varies from 85 MPa in the t = 6.35 mm to 150 MPa in the t = 15 mm thickness. Furthermore, wider residual stress distribution is observed as the pipe wall thickness increases.

For all cases, compressive axial residual stresses for about 90% to 100% of the yield strength of the weldment is achieved in the weld centre line, which doesn't vary much with changes in pipe wall thickness.

Effects of the weld groove angle

Three angles of $\theta = 45^{o}, \theta = 60^{o}$ and $\theta = 70^{o}$ in a V type groove, which is the most commonly used groove shape, were studied here. Other geometrical and welding parameters remained fixed in these analyses.

It is clearly observed that the weld groove angle have no meaningful effect on the hoop residual stresses both on the outer and inner surfaces of the weld joint. In the following, the axial residual stress distributions of the dissimilar joints on the inner and outer surfaces of the pipes are shown in Figures 16 and 17, respectively.

Weld groove angle has minor effects on peak tensile axial residual stresses on the inner surface. Increasing in the weld groove angle leads to the higher compressive residual stresses on the carbon steel side, but has very small effect on the axial stresses in the stainless steel side.

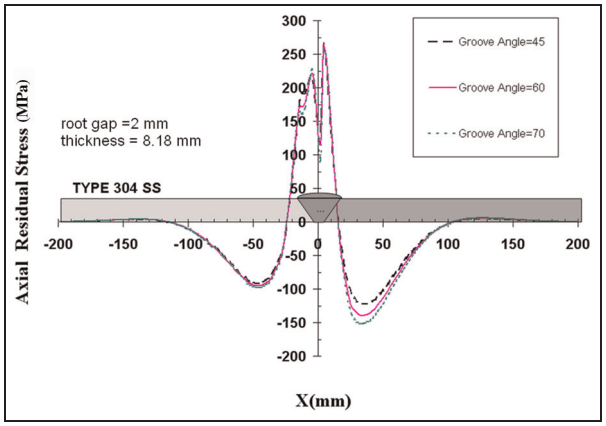

Figure 16. Axial residual stresses on the inner surface for joints with different weld groove angles.

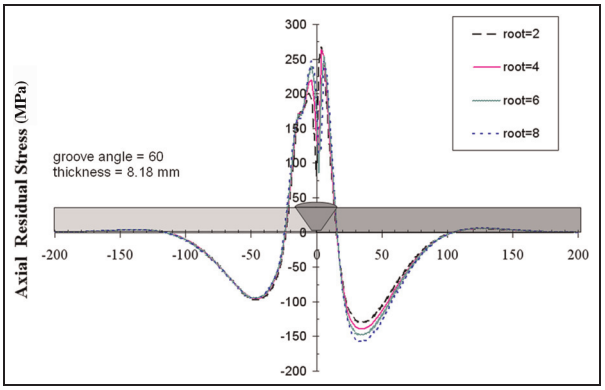

Figure 18. Axial residual stresses on the inner surface for joints with different root openings.

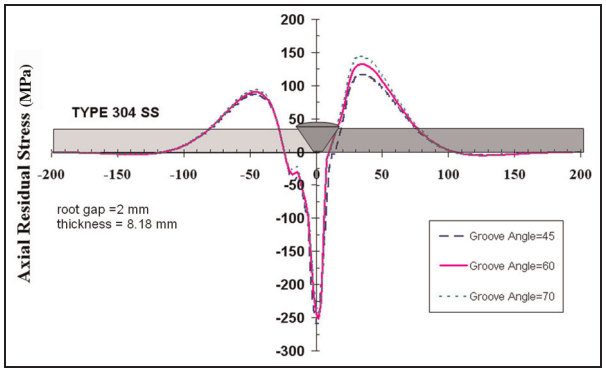

Figure 17. Axial residual stresses on the outer surface for joints with different weld groove angles.

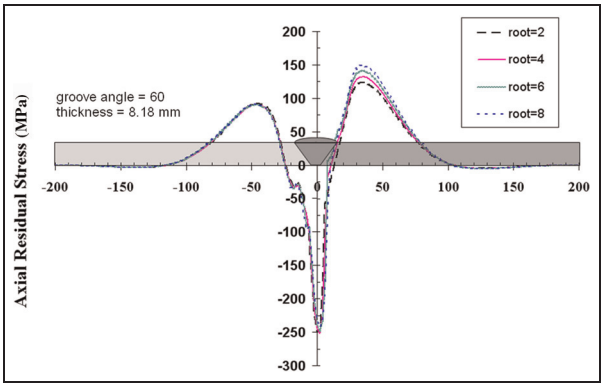

Figure 19. Axial residual stresses on the outer surface for joints with different root opening distances.

On the outer surface of the dissimilar joints, a reverse trend is observed in comparison with the inner surface. Tensile residual stresses on the carbon steel side are increased by increasing the weld groove angle and no changes are observed on the stainless steel side by changing the groove angle.

Effects of the root opening

In this part, to study the effects of the root distances on the welding residual stresses in dissimilar joints, four different root opening distances of 2, 4, 6 and 8 mm were investigated.

It is observed that the root opening distance has minor effects on hoop residual stresses. Figures 18 and 19 show the axial residual stress distributions on the inner and outer surfaces of the pipes for different root opening distances.

By increasing the root opening distances, no significant changes are observed on the stainless steel side. On the carbon steel side, the compressive axial residual stresses on the inner surface and the tensile axial residual stresses on the outer surface are increased by increasing the root opening distance.

Concluding remarks

In this study, a 3D finite element model was developed considering the phase transformation for estimating the welding residual stresses in dissimilar welded pipes fabricated from A106-B carbon steel and A240 TP304 stainless steel by multi-pass arc welding technique.

The residual stress distributions were compared with measured data presented by Deng for similar butt-welded pipes from SUS304steel. FE results for a dissimilar weld joint were also compared with the measured data by the hole drilling method. Good correspondence between FE results and experimental data observed, infer that the computational procedure developed in this study is an efficient method for residual stress prediction in dissimilar welds of thin wall pipes experience martensitic transformation. The following conclusions may be made based on the results obtained in this study.

- Shrinkage in the hoop direction due to weldment solidification creates axial residual stresses with bending profile type through the thickness in thin walled welded pipes.

- Differences between the material properties of two sides of the dissimilar joints make asymmetric distribution of residual stresses.
- By increasing the pipe thickness, tensile axial residual stresses on the inner surface of the dissimilar joint decreased on the stainless steel side, but only a small variation was observed on the carbon steel side.
- The compressive axial residual stresses on the inner surface and the tensile axial residual stresses on the outer surface increased by increasing the pipe wall thickness especially on the carbon steel side.
- The compressive hoop stresses on the inner surface increased by increasing the pipe wall thickness.
- The weld groove angle and root opening distance have no meaningful effect on the hoop residual stresses both on the inner and outer surfaces of the weld joint.
- Increasing of the weld groove angle and root opening distance lead to higher compressive axial stresses on the inner surface and higher tensile axial stresses on the outer surface, only on the carbon steel side.

Funding

This research received no specific grants from any funding agency in the public, commercial or not-for-profit sectors.

References

1. Tso-Liang T, Peng-Hsiang C and Wen-Cheng T. Effect of welding sequences on residual stresses. *J Comput Structs* 2003; 81: 273–286.
2. Joseph A, Raib-Sanjai K, Jayakumara T, et al. Evaluation of residual stresses in dissimilar weld joints. *J Pressure Vessels Piping* 2005; 82: 700–705.
3. Peng-Hsiang C and Tso-Liang T. Numerical and experimental investigations on the residual stresses of the butt-weld joints. *J Comput Mater Sci* 2004; 29: 511–522.
4. Goldak J, Chakravarti A and Bibby M. A new finite element model for welding heat source. *Metall Trans B* 1984; 15: 299–305.
5. Goldak J *Modeling thermal stresses and distortions in welds*. Ohio: ASM International, 1990, pp.71–82.
6. Mochizuki M, Hayashi M and Hattori T. Numerical analysis of welding residual stress and its verification using neutron diffraction measurement. *J Engng Mater Technol* 2000; 122: 98–104.
7. Elena S and Mihaela I. FEM application on dissimilar metals welding. *Welding equipment and technology* 2005, 250–263.
8. Akbari D and Sattari-Far I. Effect of the welding heat input on residual stresses in butt-welds of dissimilar pipe joints. *J Pressure Vessels Piping* 2009; 86: 769–776.
9. Deng D and Murakawa H. Numerical simulation of temperature field and residual stress in multi-pass welds in stainless steel pipe and comparison with experimental measurements. *J Computat Mater Sci* 2006; 37: 269–277.
10. ASTM E837, Standard test method for determining residual stress by the hole drilling strain gauge method, 1995.
11. Brickstad B and Josefson B. A parametric study of residual stresses in multi-pass butt-welded stainless steel pipes. *J Pressure Vessels Piping* 1998; 75: 11–25.
12. Goldak K, Chakaravarti A and Bibby M. A new finite element model for welding heat sources. *J Metallurgical Mater Trans* 1984; 15B: 299–305.
13. ANSYS User's manual, V10, Swanson analysis system Inc., 2004.
14. Fenggui L. Modeling and finite element analysis on GTAW arc and weld pool. *J Comput Mater Sci* 2004; 29: 371–378.
15. Sharma RC. *Principles of heat treatment of steel*. New Age Publishers, 2007.
16. Deng D and Murakawa H. Prediction of welding residual stress in multi-pass butt-welded modified 9Cr–1Mo steel pipe considering phase transformation effects. *J Comput Mater Sci* 2006; 37: 207–219.
17. Paradowska A, Price J, Ibrahim R, et al. The effect of heat input on residual stress distribution of steel welds measured by neutron diffraction. *J Achievements in Mater Mfg Engng* 2006; 17: 385–388.